Impact of the local atomic structure on the thermal conductivity of amorphous Ge2Sb2Te5

Mohammed Guerboub, Steve Dave Wansi Wendji, Carlo Massobrio, Assil Bouzid, Mauro Boero, Guido Ori, Evelyne Martin

Impact of the local atomic structure on the thermal conductivity of amorphous $Ge_2Sb_2Te_5$

Mohammed Guerboub[a),1] Steve Dave Wansi Wendji[a),1] Carlo Massobrio,[1] Assil Bouzid,[2] Mauro Boero,[1] Guido Ori,[1] and Evelyne Martin*[3]

[1)]*Université de Strasbourg, CNRS, Institut de Physique et Chimie des Matériaux de Strasbourg, UMR 7504, Strasbourg F-67034, France*

[2)]*Institut de Recherche sur les Céramiques (IRCER), CNRS UMR 7315, Université de Limoges, Centre Européen de la Céramique, 12 rue Atklantis, 87068 Limoges*

[3)]*Université de Strasbourg, CNRS, Laboratoire ICube, UMR 7357, F-67037 Strasbourg, France*

(*Electronic mail: evelyne.martin@unistra.fr)

(Dated: 24 October 2023)

[a)] M. Guerboub and S. D. Wansi Wendji contributed equally to this work and they are listed here following the alphabetic order.

Impact of the local structure on the thermal conductivity of *a*GST

Thermal properties are expected to be sensitive to the network topology and yet no clearcut information is available on how the thermal conductivity of amorphous systems is affected by details of the atomic structure. To address this issue we use as a target system a phase change amorphous material (GST, i.e. $Ge_2Sb_2Te_5$) simulated by first-principles molecular dynamics (FPMD) combined with the approach-to-equilibrium molecular dynamics technique (AEMD) to access the thermal conductivity. Within density-functional theory (DFT), we employed two models sharing the same exchange-correlation functional but differing in the pseudopopotential (PP) implementation (namely, Trouiller-Martins, TM and Goedecker, Teter and Hutter, GTH). They are both compatible with experimental data and yet the TM PP construction results in a Ge tetrahedral environment largely predominant over the octahedral one, while the proportion of tetrahedra is considerably smaller when the GTH PP is used. We show that the difference in local structure between TM and GTH models impacts the vibrational density of states while the thermal conductivity does not feature any appreciable sensitivity to such details. This behavior is rationalized in terms of extended vibrational modes.

I. INTRODUCTION

Phonons act in crystals as heat carriers experiencing scattering events. However, at short scale, some phonons behave ballistically, their mean free path becoming larger than the dimensions of the system. This results in a reduction of the total thermal conductivity, as observed experimentally and theoretically[1–4]. The impact of downscaling on the thermal conductivity of amorphous materials and glasses is more elusive. The thermal conductivity is reduced at short scales in amorphous silicon, as shown by experiments[5] and modeling[6]. In addition, first-principles molecular dynamics (FPMD) simulations of thermal transients (approach-to-equilibrium molecular dynamics, AEMD hereafter) have evidenced a reduction of thermal conductivity in other disordered materials (amorphous $GeTe_4$[7], $Ge_2Sb_2Te_5$[8] and SiO_2[9]). A view commonly accepted for the heat transport in amorphous materials includes propagative heat carriers, the propagons (equivalent to phonons in the crystals) along with heat carriers that do not have well defined wave-vectors but are extended, the diffusons, and localized vibrations, the locons[10]. The reduction of thermal conductivity mentioned above highlights the impact of extended modes in the heat transport of disordered materials. Yet, it is still unclear if the thermal conductivity is sensitive to the local atomic environment, and if so, by which amount it is modified. In principle, this can be achieved by realizing different model systems of the same material, the difference being nature and connectivity of their building motifs. While this strategy is somewhat cumbersome to implement experimentally, it falls entirely within the capabilities of quantitative atomic-scale modelling. This is exactly the guideline pursued in this paper, in which we focus on amorphous $Ge_2Sb_2Te_5$ (*a*GST), a phase-change material used in resistive memory devices for in-memory computing[11] or as reconfigurable light management solution in nanophotonics[12]. In a previous work[13], we have studied the structure of bulk *a*GST via FPMD by implementing a thermal cycle on a periodic box of 144 atoms. Several choices of the pseudopotential (PP) constructions within the PBE[14] and BLYP[15,16] exchange-correlation functionals were adopted. The combination of the BLYP exchange and correlation functional with the Troullier-Martins (TM)[17] PP resulted in an excellent agreement between the calculated and measured total neutron structure factor, leading to a predominance of Ge atoms in tetrahedral environnment. An entirely different structure, yet still compatible with experiments in terms of total neutron structure factor, was obtained by employing BLYP along with GTH[18] PPs, the proportion of Ge in tetrahedra decreasing from 69% (TM) to 22% (GTH). As a first purpose of this work, we intended to rule out size effects and confirm (or disprove) the difference of local structure be-

tween TM and GTH by considering a larger supercell made of 504 atoms (112 Ge, 112 Sb and 280 Te). To this end, we have constructed a new GST-GTH model and extended the trajectory of the GST-TM already available in Ref. 8. Persisting structural differences are exploited to ascertain the sensitivity of the vibrational density of states and of the thermal conductivity to the atomic scale organization of *a*GST. Therefore, a second, major outcome of our work is a fundamental insight into the relationship between a set of macroscopic properties and the network structure of a PCM material. We are able to exploit two available atomic structures for *a*GST, each one corresponding to a network organization in line with contrasting experimental descriptions (defective octahedra *vs* tetrehedra), to assess their impact on a fundamental macroscopic thermal property.

The paper is organized as follows. As a necessary prerequisite to the understanding of the issues inherent in the structural determination *a*GST, we briefly recall in Sec. II the context of the long lasting debate on the relative importance of tetrahedral *vs* octahedral basic units. In Section III, we provide a description of our calculation methodology and we introduce the FPMD models. Section IV is devoted to the analysis of their structure. In Section V, an analogous comparative analysis is performed for the vibrational properties. Conclusions are contained in Section VI.

II. THE ATOMIC STRUCTURE OF AMORPHOUS GST: TETRAHEDRAL *VS* OCTAHEDRAL BONDING GEOMETRIES

Having established that our investigation is fully rooted on the existence of different kinds of networks for *a*GST, it is worth contextualizing it within the longstanding debate on the relative importance of tetrahedral *vs* octahedral structural motifs. From the standpoint of modelling, we shall refer almost exclusively to structural descriptions obtained in the framework of FPMD, either employed as a self-contained tool of quantitative prediction or in combination with experimentally guided structural refinements as reverse Monte-Carlo (RMC). Early contributions addressing the presence of both tetrahedral (TE) and defective octahedral (DO) structural motifs were made available in Refs. 19–27. Vibrational properties were also considered in connection with the corresponding crystalline behavior.[19,22,25]

These findings have been complemented and enriched over the years by additional pieces of information focusing on the assessment of the relative percentage of TE and DO Ge sites. The predominance of octahedral sites over tetrahedral ones is a common feature of a number of independent FPMD calculations,[19–24,27–29] for which only one third of Ge atoms are in tetrahedral

geometries. Interestingly, even smaller TE Ge sites percentages are found when resorting to a Machine Learning model,[30] built within the same FPMD framework of Refs. 24 and 31. These results are not entirely in agreement with experimental evidence pointing toward more extended tetrahedral order (EXAFS, x-ray absorption fine structure) and, for the nearest neighbor distances, a concomitant sizeable overestimate affecting FPMD values.[32–34] Observed "wrong" Ge−Ge bonds are also more compatible with a tetrahedral arrangement.[35] To solve this inconsistency by invoking the notion of polymorphism in phase-change materials, Akola *et al.*[36] proposed that the as-deposited (AD) models, closer in spirit to experimental realizations, could lead to a larger number of tetrahedral sites with respect to melt-quenched (MQ) ones, thereby promoting shorter FPMD distances. As touched upon in Sec. I, an alternative manner to recover shorter interatomic distances while extending the impact of tetrahedral configuration for MQ structure was presented in Ref. 13 (this reference contains also a detailed comparison with previous structural data obtained from experiments and FPMD calculations). In that work, a specific choice for the description of the nonlocal part in the Troullier-Martins[17] pseudopotential construction for Ge resulted in unprecedented agreement for the total neutron structure factor and the interatomic distances. Ge atoms are found in a predominant tetrahedral network coexisting with a non-negligible fraction of Ge in defective octahedra. However, it was argued that this atomic-scale picture is not consistent with Raman spectral features, tetrahedral coordination arising from Ge atoms being absent in experiments and first-principles calculations.[25] Overall, while an unambiguous structural determination for *a*GST remains elusive, it is worth mentioning that anomalous x-ray scattering[37] focussing on both short and intermediate range order have somewhat reconciled TE and DO views on the Ge coordination, both manifesting themselves in the experimental patterns with close percentages.

On the theoretical side, it appears that refinements in the DFT-based description could be instrumental to an improved structural assessment. With this purpose in mind, inclusion of dispersion forces has attracted considerable attention for both amorphous GeTe and GST.[38–40] Ref. 41 provides a very recent review of state-of-the-art ideas and open issues on the atomic structure of amorphous GeTe and GST.

Finally, given the above context, we reiterate that one of the strength of the present work is to take advantage of two atomic structure for *a*GST, both compatible with distinct experimental determinations and produced in a concomitant fashion, in order to ascertain their sensitivity to a specific macroscopic thermal property, i.e. the thermal conductivity.

III. METHODOLOGY OF CALCULATIONS

Calculations were performed within the Car-Parrinello[42] method as implemented in the developers version 4.3 of the CPMD code[43]. We selected for the exchange-correlation part of the Kohn-Sham total energy functional the exchange formula proposed by Becke[15] and the correlation one of Lee, Yang and Parr[16] (BLYP). The valence-core interactions are described by either numerical norm-conserving TM[17] or by analytical norm-conserving GTH[18] PPs. For the choices inherent in the Kleinmann-Bylander expression of the local and non-local parts of the pseudopotentials we refer to the rationale given in Ref. 13. Valence electrons are represented by a plane-wave basis set compatible with periodic boundary conditions, with a cutoff of 30 Ry, and the sampling of the Brillouin zone is limited to the Γ point. A fictitious electron mass of 500 a.u. and a time step Δt = 0.12 fs (5 a.u.) are chosen to ensure optimal numerical conservation of the constants of motion. In all canonical NVT simulations, the ionic temperature was controlled with a Nosé-Hoover[44–46] thermostat chain,[47] whereas for the fictitious electronic kinetic energy we used a Blöchl-Parrinello thermostat[48] with a target kinetic energy depending on the ionic temperature.

Our models made of N= 504 atoms (termed concisely hereafter 504-TM and 504-GTH, meaning 504-TM model and 504-GTH model respectively) have an elongated shape (20.3×20.3×40.6 Å^3) designed to study thermal transport as a function of the length along the z direction via the AEMD technique as explained in Section III. This non-cubic shape remains fully compatible with the objective of representing the structure of a bulk material. Periodic boundary conditions are applied in the three directions. Thermal cycles are employed to randomize the initial atomic configuration and to quench afterwards into the amorphous state. For the models containing 144 atoms, we implemented in Ref. 13 five trajectories of respectively 40 ps at T = 300 K, 20 ps at T = 600 K, 70 ps at T = 900 K, 50 ps at T = 600 K and 42 ps at T = 300 K. The 504-TM model is the same as model D2 of Ref. 8. However, the trajectory at T= 300 K has been extended by 35 ps to increase the statistical accuracy of the average properties. The initial configuration used for the 504-GTH is taken from the atomic positions of 504-TM relaxed within the BLYP-GTH computational setup. Then, a thermal ramp has been implemented as follows : T= 10 K (5 ps), T=100 K (5 ps), T=300 K (8 ps), T=600 K (10 ps) and T=900 K (8 ps). At T= 900 K, the mean square displacements of the Ge, Sb and Te atoms reported in Fig. 1 lead to diffusion coefficients larger than 10^{-5} cm^2 s^{-1} (Table I). These values ensure loss of memory of the initial configuration and effective randomization. Quench to room temperature occurred via a first step of 30 ps at T = 600

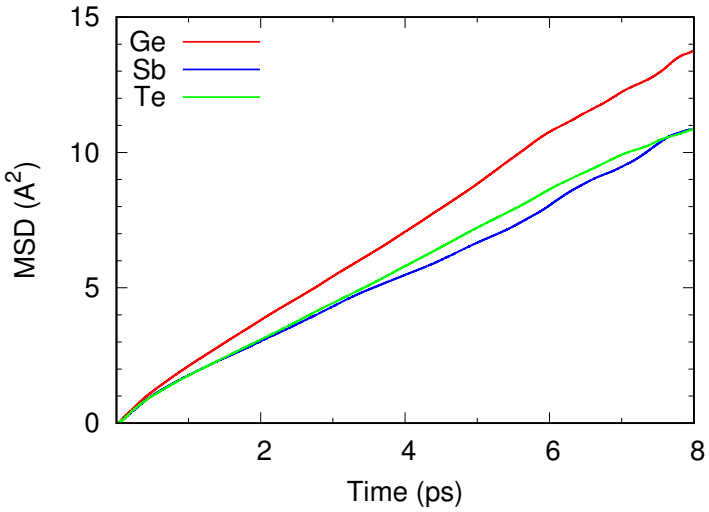

FIG. 1. Mean square displacement of Ge (red line), Sb (blue line) and Te (green line) in 504-GTH at T = 900 K.

TABLE I. Diffusion coefficients at T = 900 K

	504-GTH	504-TM
D_{Ge} (cm^2 s^{-1})	2.8×10^{-5}	2.2×10^{-5}
D_{Sb} (cm^2 s^{-1})	2.2×10^{-5}	1.8×10^{-5}
D_{Te} (cm^2 s^{-1})	2.3×10^{-5}	1.2×10^{-5}

K followed by a second step of 35 ps at T = 300 K. Statistics were collected on this final part of the thermal cycle.

IV. STRUCTURAL PROPERTIES

A. Partial pair correlation functions

Partial pair correlation functions $g_{\mathrm{GeGe}}(r)$, $g_{\mathrm{GeSb}}(r)$, $g_{\mathrm{GeTe}}(r)$, $g_{\mathrm{SbSb}}(r)$, $g_{\mathrm{SbTe}}(r)$ and $g_{\mathrm{TeTe}}(r)$ for the four models considered (144-TM, 504-TM, 144-GTH, 504-GTH) are reported in Fig. 2, with the corresponding bond lengths and coordination numbers given in Table II.

Focussing on $g_{\mathrm{GeGe}}(r)$, $g_{\mathrm{GeSb}}(r)$ and $g_{\mathrm{SbSb}}(r)$ one observes more regular profiles for 504-TM and 504-GTH compared to the smaller size, indicative of noise reduction. In the case of $g_{\mathrm{GeGe}}(r)$ the amplitude of the first peak, corresponding to homopolar Ge-Ge bonds, is significantly more intense for 504-TM than for 504-GTH, with a ratio between the relative heights increased in com-

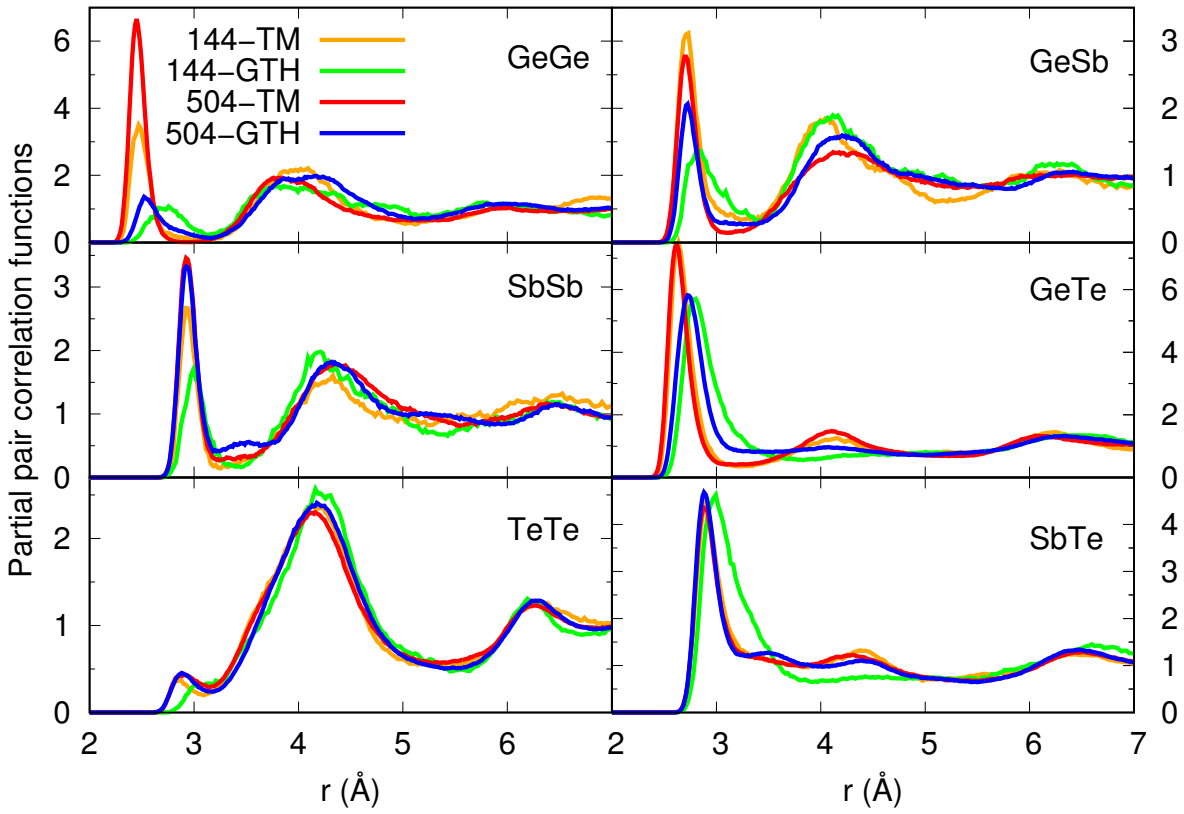

FIG. 2. Partial pair correlation functions of amorphous $Ge_2Sb_2Te_5$. The color codes for the four models are as follows: 504-TM: red, 504-GTH: blue, 144-TM: orange and 144-GTH: green.

parison with 144-TM and 144-GTH. The position of this peak (2.46 Å for 504-TM vs 2.47 Å for 144-TM, 2.54 Å for 504-GTH vs 2.75 Å for the 144-GTH) confirms the better performances of TM when compared to GTH for this specific feature, while the increase in size has the effect of approaching the GTH value to the experimental data (2.47 Å). Turning to $g_{\mathrm{GeSb}}(r)$, we can observe that the positions of the first peak (see also Table II) for TM and GTH models are closer in the larger boxes (2.72 Å for 504-TM vs 2.74 Å for 504-GTH) as well as their heights. While the TM approach is in better agreement with experiments, this is a further sign of increased reliability of GTH when compared to TM within the DFT-FPMD framework. In the case of $g_{\mathrm{GeTe}}(r)$, the first peak is located at a larger distance for both 504-GTH and 144-GTH models, although a shift toward smaller values is present in the case of the larger size (2.74 Å for the 504-GTH vs 2.80 Å for the 144-GTH). TM values compare very well with experiments (see Table II). The partial pair correlation functions $g_{\mathrm{SbSb}}(r)$, $g_{\mathrm{SbTe}}(r)$ and $g_{\mathrm{TeTe}}(r)$ obtained via 504-TM and 504-GTH are very

TABLE II. Bond lengths ($r_{\alpha\beta}$) and partial coordination numbers ($n_{\alpha\beta}$) extracted from the partial pair correlation functions $g_{\alpha\beta}(r)$ of amorphous $Ge_2Sb_2Te_5$. Experimental results are from Refs. 49 and 50. The results of the four models are reported: 504-TM, 504-GTH and the two models of Ref. 13, 144-TM and 144-GTH. Bond lengths are taken as the position of the first maxima of the pair correlation functions. The coordination numbers $n_{\alpha\beta}$ are obtained by integration of the pair correlation functions up to the first minima. $n_{\alpha\beta}$ are given in the table together with the position of the first minimum $r_{\alpha\beta}^{\min}$ at which they were determined (notation: $n_{\alpha\beta}@r_{\alpha\beta}^{\min}$). For a comparison with previous FPMD data obtained in Refs. 20, 22, and 29 see Ref. 13

	Exp.		144 atoms		504 atoms	
	Ref. 49	Ref. 50	144-TM	144-GTH	504-TM	504-GTH
r_{GeGe} (Å)		2.47	2.47	2.75	2.46	2.54
r_{SbSb} (Å)			2.92	3.00	2.95	2.95
r_{TeTe} (Å)					2.95	2.89
r_{GeSb} (Å)			2.73	2.82	2.72	2.74
r_{GeTe} (Å)	2.61	2.63	2.66	2.80	2.63	2.74
r_{SbTe} (Å)	2.85	2.83	2.89	3.00	2.89	2.89
n_{GeGe}		0.6±0.2	0.42@3.1Å	0.29@3.1Å	0.63@2.9Å	0.26@3.1Å
n_{SbSb}			0.41@3.2Å	0.36@3.4Å	0.55@3.3Å	0.54@3.2Å
n_{TeTe}			0.18@3.1Å	0.20@3.2Å	0.27@3.1Å	0.28@3.2Å
n_{GeSb}			0.59@3.3Å	0.43@3.3Å	0.41@3.1Å	0.31@3.1Å
n_{GeTe}		3.3±0.5	3.02@3.2Å	4.27@3.5Å	2.75@3.1Å	3.27@3.3Å
n_{SbTe}		2.8±0.5	2.99@3.4Å	3.85@3.4Å	3.19@3.5Å	2.60@3.3Å

close over the whole range of distances with the exception of the first minimum in the $g_{\mathrm{SbSb}}(r)$, lower in 504-TM. A slight overestimate is found when comparing Sb-Te interatomic distances (for both 504-TM and 504-GTH) to experimental values. We conclude that the partial pair correlation functions calculated with N= 504 within two different frameworks (TM and GTH) are less dissimilar than what they were found to be for N= 144 (see Ref. 13). Yet, this confirms the better performances of the TM PPs as implemented in Ref. 13 for this class of systems.

B. Coordination number and local environment

The main effect of the larger size (504-GTH) in comparison with the smaller 144-GTH counterpart is a better agreement with available measurements for n_{GeTe} and n_{SbTe} (3.27 vs 3.3±0.5 for n_{GeTe} and 2.60 vs 2.8±0.5 for n_{SbTe}). For these coordination numbers, TM models have comparable accuracy. Concerning n_{GeGe}, a very good agreement with experimental data is found for 504-TM (0.63 vs 0.6±0.2), while n_{GeGe} values of 144-GTH and 504 -GTH are very close and differ substantially from experiments. Table III provides the evolution of n_{GeGe} and n_{GeSb} during the ramp down of the thermal cycle for 504-GTH. The concentration of homopolar Ge-Ge bonds at T = 900 K reduces by a factor of two upon quenching, while a less pronounced decrease of the number of Ge-Sb bonds is observed. Similar trends are obtained for the other models (504-TM, 144-TM and 144-GTH).

TABLE III. Evolution of n_{GeGe} and n_{GeTe} during the quench of 504-GTH. The position of the first minimum at which they were determined is given following the same convention as in Table II

	T = 300 K	T = 600 K	T = 900 K
n_{GeGe}	0.26@3.1Å	0.32@3.1Å	0.52@3.1Å
n_{GeSb}	0.31@3.1Å	0.36@3.2Å	0.43@3.3Å

Finally, the coordination numbers n_{SbSb} and n_{TeTe} obtained via TM and GTH do not change appreciably with the system size, while n_{GeSb} remains higher for both (N= 144 and N= 504) TM models. These considerations reflect the shapes of the partial pair correlations functions and are globally in line with the better quality of TM models in comparison with experiments.

A global view on the distribution of the coordination numbers for Ge, Sb and Te is shown in Fig. 3. The local environnement of Sb and Te is very similar within the TM and the GTH schemes at N=504, as an indication that the differences observed at N=144 decrease with increasing size. 504-TM and 504-GTH feature, as 144-TM, a dominant threefold coordination for Sb and twofold for Te. Ge atoms are mostly fourfold coordinated in all realizations. Worth of interest is the change in the nature of the second most frequent population for Ge. In 144-GTH there was a significant amount (34 %) of fivefold coordinated Ge atoms, while threefold atoms are instead found in a similar proportion (32 %) in 504-GTH. Another difference appears when looking at the chemical species connected to fourfold coordinated Ge atoms, shown in Table IV. Whereas Ge-Ge and Ge-Sb bonds are observed for all cases, for example taking the form of $GeTe_3$ or $SbTe_3$ structural

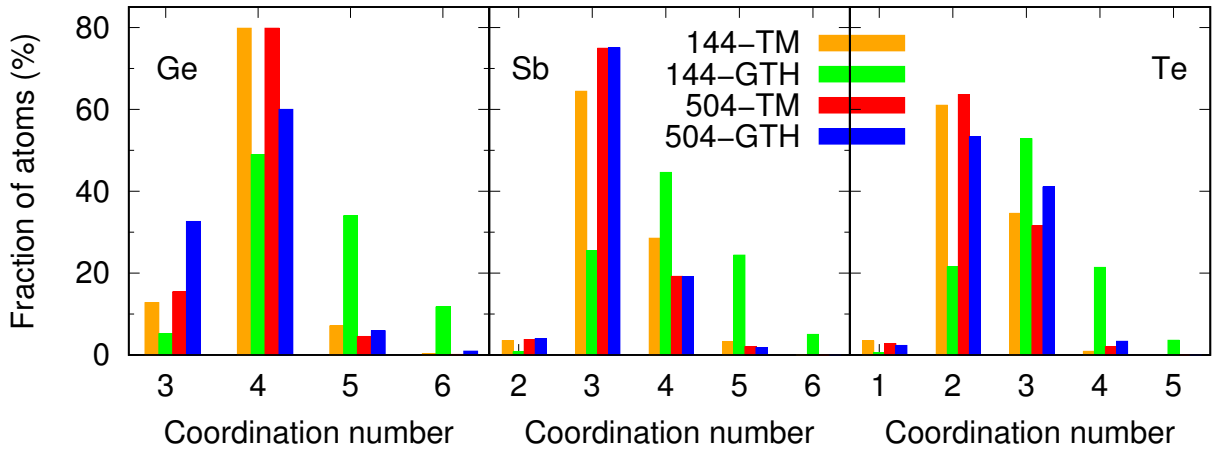

FIG. 3. Fraction of *n*-fold Ge, Sb and Te atoms (*n*=1 to 6). The color codes for the four models are as follows: 504-TM: red, 504-GTH: blue , 144-TM: orange, 144-GTH: green.

units, their proportion is larger with the TM models (144-TM and 504-TM), since only 26 and 16 % of the fourfold coordinated Ge do not form a bond with a Ge or a Sb atom, to be compared with $\sim$ 50 % for the GTH models. These findings are in agreement with previous evidence linking the occurrence of tetrahedral motifs and the presence of Ge−Ge and Ge−Sb connections.[21,24,27,28]

TABLE IV. Decomposition of the fourfold Ge environment in structural units with their chemical identity. For each structural unit, we give its relative weight (percentage) with respect to the total number of Ge atoms fourfold connected

Fourfold-coord. Ge (%)	504-GTH	504-TM	144-GTH	144-TM
Te_4	43.7	16.2	46.5	26.2
$GeTe_3$	19.2	35.4	11.5	22.2
$SbTe_3$	19.7	19.0	23.0	26.7
$GeSbTe_2$	9.8	14.5	13.0	8.1
Ge_2Te_2		5.6		
Sb_2Te_2	7.7	5.6	6.0	9.0
Ge_2SbTe				7.8
Ge_3Te		3.6		

We have seen that Ge atoms are mostly fourfold coordinated for both sizes regardless of the

choice for the pseudopotential scheme. The question arises on whether or not this feature means a similar network organization, as it could be tentatively concluded. For N = 144, the results of Ref. 13 showed that this was not the case since the proportion of Ge atoms in tetrahedral units (69 vs 22 % for TM and GTH, respectively) was a major difference in the Ge environment between the BLYP-TM and BLYP-GTH schemes. This was obtained by resorting to the integral of the order parameter[51] $q = 1 - \frac{3}{8}\sum_{i>k}(\frac{1}{3} + \cos\theta_{ijk})^2$ between 0.8 and 1. The same analysis performed for N = 504 gives 69% of tetrahedral Ge units for 504-TM model and 37 % for 504-GTH one, confirming the stronger tetrahedral character of the network obtained by adopting the TM BLYP pseudopotential formulated in Ref. 13. These values can be compared to those obtained in Ref. 36 where as-deposited (AD) and melt-quenched (MQ) models were created to demonstrate that the former method is more effective in favoring tetrahedral bonding geometries than the latter. Values obtained in Ref. 36 for tetrahedral coordination are 58% for AD and 36% for MQ, both smaller than the corresponding 69% reported above for 504-TM within MQ modelling.

Ever since the first FPMD modelling efforts on *a*GST, rings structures have been considered to play an important role in driving the crystallization process.[24] Our calculated distribution of primitive rings,[52] reported in Fig. 4, is normalized on the total number of rings containing between three and ten atoms. Considering the fourfold rings, the ABAB configuration with A being a Ge or Sb atom, and B a Te one are more numerous (85%) in 504-GTH than in 504-TM (74%) (see insets of Fig. 4). This is consistent with the well known tendency of tetrahedral configurations to favor Ge−Ge homopolar bonds,[21,28] as confirmed by the data presented in Tab. IV.

To close this section, a final word is in order on the comparative analysis of TM and GTH systems for differents sizes (N= 504, N= 144). Based on the structure of the various GST networks considered here, it appears that TM and GTH schemes are closer when the system size is larger (N= 504 against N= 144) and yet an unambiguous difference in terms of overall structural organization does persist.

C. Total structure factor and best choice for reproducing experimental data

In Fig. 5 the total neutron structure factors $S_T(k)$ obtained via 504-TM and 504-GTH are compared to what was previously obtained for 144-TM and 144-GTH as well as to experiments ($S_T^{\mathrm{Exp}}(k)$). The structure factors are obtained from the Fourier transform of the pair correlation functions. $S_T(k)$ does not differ significantly when considering 504-TM and 144-TM, both ex-

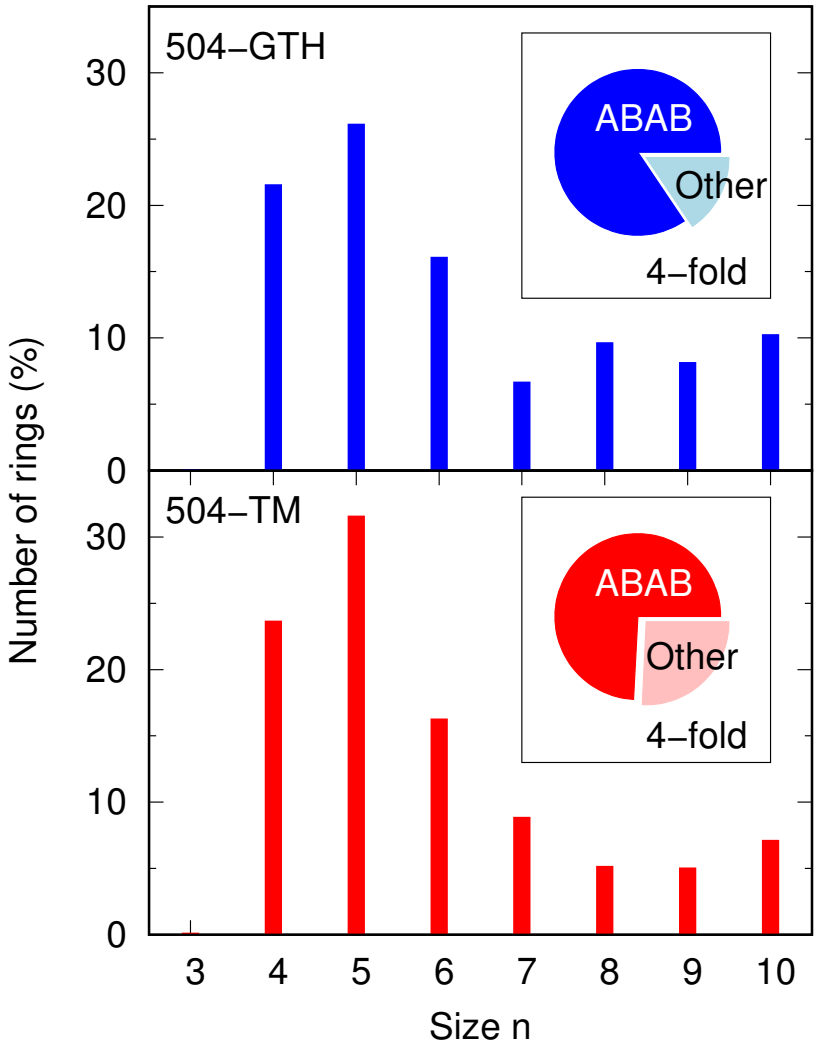

FIG. 4. Distribution of rings of size n containing up to $n = 10$ atoms. For each model, the percentage of fourfold rings found in ABAB (A=Ge or Sb and B=Te) configuration is given in the inset.

hibiting peaks positions and intensities very close to the experiments. A moderate shift to lower values of k is observed for the peak at ~ 5 Å^{-1}. Turning to the GTH results, $S_T(k)$ is substantially improved in 504-GTH with respect to 144-GTH since the second and the third peaks are better reproduced, the shoulder around 4.5 Å^{-1} has a smaller amplitude and the fourth peak is shifted to higher values in closer agreement with the experiments. The intensity around 1 Å^{-1} remains somewhat underestimated, with the best agreement found for 144-TM. Interestingly, when comparing the TM-based and GTH-based results, differences are alleviated by the larger size, leading

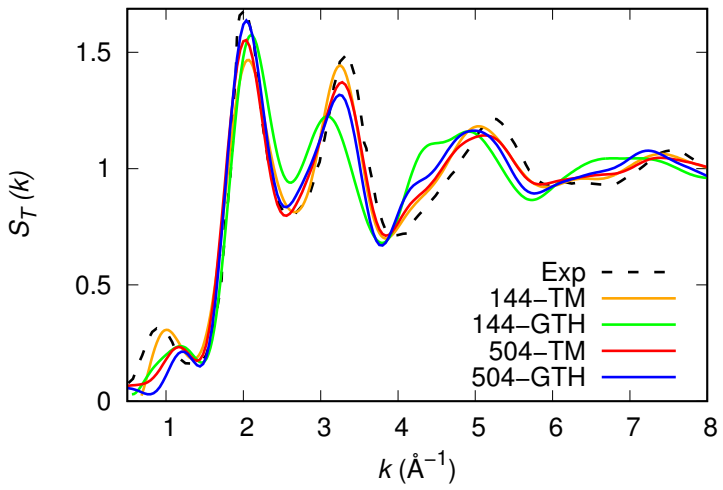

FIG. 5. Calculated (solid lines) and experimental (dashed line) neutron structure factor $S_T(k)$ of amorphous $Ge_2Sb_2Te_5$. The color codes for the four models are as follows: 504-TM: red, 504-GTH: blue, 144-TM: orange and 144-GTH: green.

to the observation that $S_T(k)$ is reproduced to an acceptable extent by both 504-TM and 504-GTH, with TM remaining preferable over GTH. This rationale is substantiated by the calculation of the Wright parameter[53] R_χ:

$$R_\chi = \left(\frac{\sum_i \left[S_T^{\mathrm{Exp}}(k_i) - S_T(k_i) \right]^2}{\sum_i \left[S_T^{\mathrm{Exp}}(k_i) \right]^2} \right)^{1/2} \tag{1}$$

that is inversely proportional to the degree of agreement with the experimental values $S_T^{\mathrm{Exp}}(k)$. The values for the four systems are given in Table V. While the BLYP-TM recipe remains the best performing, for larger size the discrepancy affecting the GTH-based result decreases significantly. TM remains the best choice for reproducing experimental data on the structure of bulk amorphous

TABLE V. Wright parameter R_χ (%) for the four GST models.

DFT recipe	144 atoms	504 atoms
BLYP-TM	6.8	9.2
BLYP-GTH	12.9	11.5

GST, pointing to a predominant Ge-centered tetrahedral organization. The size of the supercell (504 vs 144 atoms) has a moderate effect on the comparative performances of the two schemes, TM vs GTH, in regard of their adequacy to describe quantitatively the structure of bulk *a*GST.

V. VIBRATIONAL PROPERTIES

A. Density of states

A first insight into the impact of the GST network organization on the vibrational properties is given by the Fourier transform of the velocity-velocity autocorrelation function, providing the vibrational density of states (vDOS) (Fig. 6).

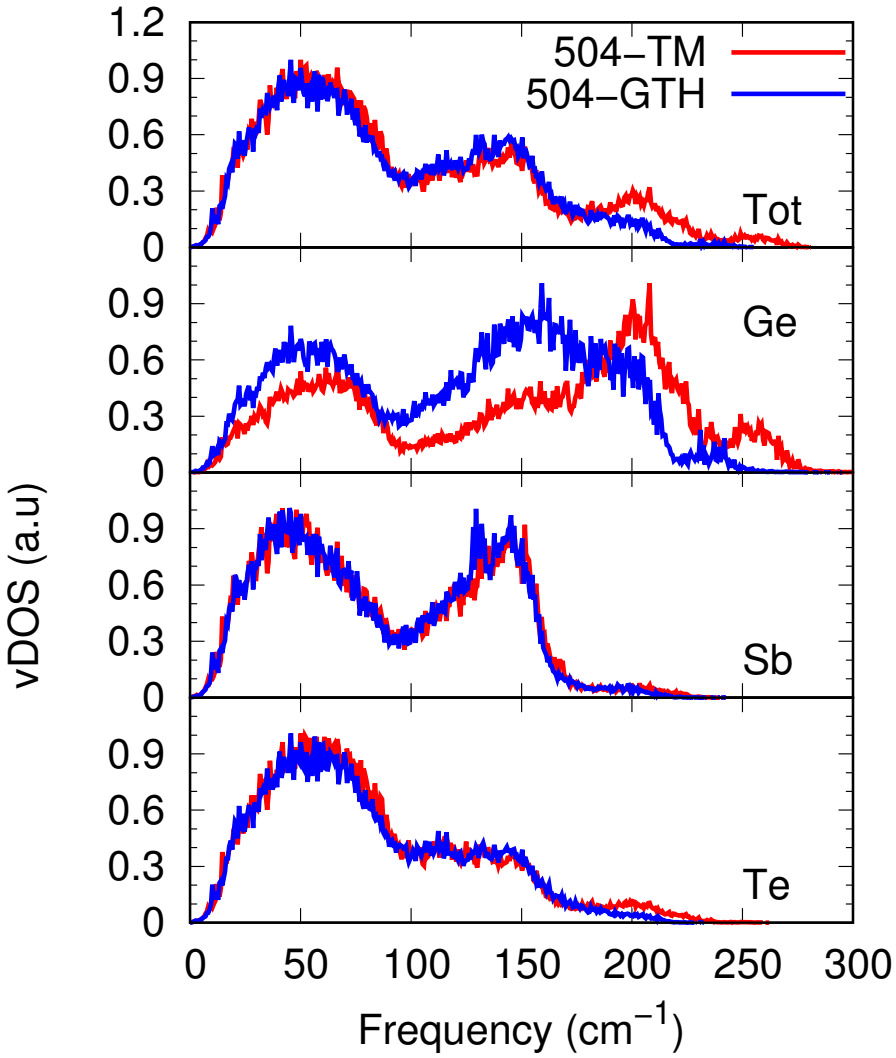

FIG. 6. Total and partial vibrational densities of states for the models 504-TM (red lines) and 504-GTH (blue lines).

The total vDOS differ at frequencies larger than 170 cm^{-1}. The contributions of Sb and Te show little sensitivity to the type of network generated by either TM or GTH PPs. The vDOS of Ge instead, features a shift at a higher frequency of the main peak for 504-TM ($\sim$ 200 cm^{-1} against $\sim$ 150 cm^{-1} for 504-GTH) together with a range of values extending up to $\approx$ 275 cm^{-1} that explains the differences observed in the total vDOS. This result is in line with the observation that the local environment of Ge is the most sensitive to the modelling framework (TM or GTH), showing that higher frequencies in the vDOS of Ge appear when Ge is mostly in the TM tetrahedral environment.

We have employed the vibrational eigenvectors (obtained by diagonalization of the Hessian) to quantify the localization of the vibrational modes by calculating the inverse participation ratio

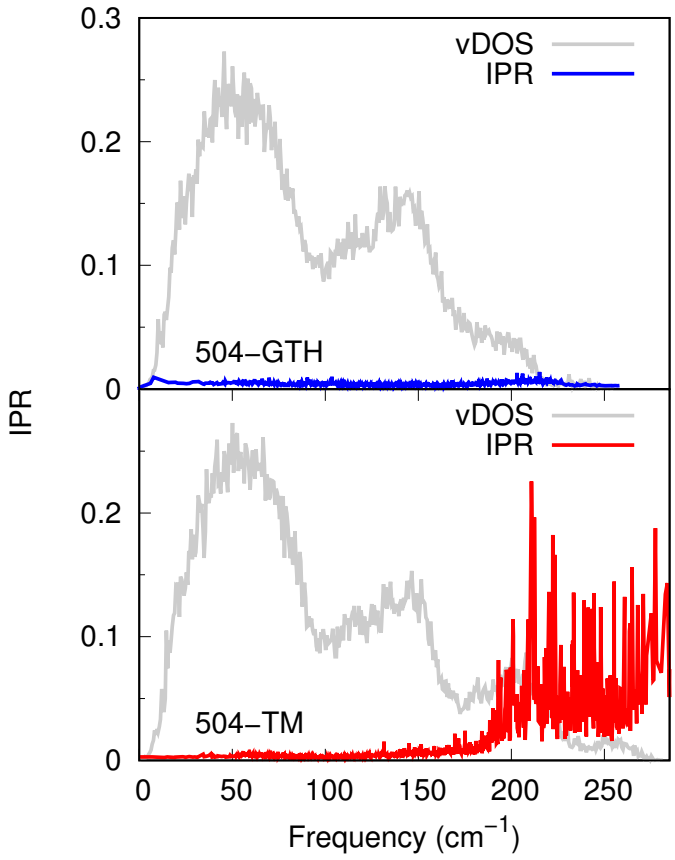

FIG. 7. Inverse participation ratio of the vibrational states for the models 504-TM (red lines) and 504-GTH (blue lines). The total vibrational DOS are reported in light grey to recall the range of frequencies involved in each case.

(IPR) defined as:[54,55]

$$\frac{1}{p_n(\omega_n)} = \left(N \sum_{i=1}^{N} \left(\|\vec{e}_i(\omega_n)\|^2 \right)^2 \right) / \left(\sum_{i=1}^{N} \|\vec{e}_i(\omega_n)\|^2 \right)^2 \quad (2)$$

for a mode of eigenvalue ω_n and eigenvector $\vec{e}_i(\omega_n)$. The IPR is equal to $1/N$ for a fully delocalized vibrational mode, while it reaches 1 at the extreme opposite (localization on a single atom). The IPR are reported for both models in Fig. 7. The IPR is significantly higher in 504-TM at high frequency, in the region where the vibrational states differ. These localized modes are not expected to contribute to the heat transport as it will appear clearly below when considering the results obtained for the thermal conductivities. The link between modes localization and Ge tetrahedral sites was already pointed out in Ref. 22.

B. Thermal conductivity

By calculating the thermal conductivity we aim at understanding the impact of the atomic structure on relevant quantities such as heat carriers (to be intended in their most general expression) not directly arising from averages over the time evolution of the atomic positions, as done up to now. To this purpose, we resort to the approach-to-equilibrium molecular dynamics (AEMD) methodology, already applied to several amorphous systems.[7–9,56,57] AEMD is based on the implementation within molecular dynamics of a particular regime of the heat equation, where periodic and transient temperature profiles evolve in one dimension. The period is fixed at the largest possible value, i.e. the direction in the z direction of the elongated supercell (hereafter called L and equal to 40.6 Å). The transient decay time τ is related to the thermal conductivity κ by the expression :

$$\kappa = \frac{L^2}{4\pi^2} \frac{\rho C}{\tau} \quad (3)$$

where $\rho = 1/V$ is the number density or inverse of the volume, and C is the heat capacity. For this quantity, the deviation γ from the Dulong and Petit $C^{\mathrm{DP}} = 3Nk_{\mathrm{B}}$ value ($C = \gamma C^{\mathrm{DP}}$) is calculated from the temperature derivative of the total energy averaged over the thermal cycle. For the TM scheme, a value of γ_{TM}=1.365±0.015 was obtained in our previous work.[8] The value obtained for the GTH scheme is γ_{GTH}=1.130±0.018.

The transient and periodic temperature profiles are established by setting up an out-of-equilibrium initial configuration via the application of two local thermostats while the periodic boundary conditions are maintained (it is the so-called phase 1). The first thermostat, at T =400 K, acts on the

atoms lying between 0 and $L/2$, while the second at T =200 K on those between $L/2$ and L. At the end of phase 1, lasting typically 5 ps, the temperature profile has a periodic form alternating between hot and cold regions, with a period equal to the length L in the z direction. The temperature profile in the range $[0-L]$, averaged during phase 1, is shown in Fig. 8.

During the transient that follows (phase 2), the temperature profile becomes sinusoidal (Fig. 8) as predicted by the heat equation, and its amplitude decreases with time. The difference of temperature between the hot block ($0 < z < L/2$) and the cold one ($L/2 < z < L$) decreases following $\exp(-t/\tau)$ as depicted in Fig. 9 on a semi-log plot.

The transient time τ and thermal conductivity κ obtained in this way for 504-TM and 504-GTM models are reported in Table VI. The error bar results from the account of several AEMD runs via extensions of the phase 1 by 5 ps. This allow reaching a new initial point of the transient regime fully decorrelated from the previous one. Within the statistical error, the thermal conductivity does not differ when comparing the two models.

This result exemplifies the intriguing behavior of the vibrational properties of amorphous materials, with local vibrational modes impacting the vDOS, while extended ones, involved in the heat transport, are insensitive to the local structural features. It is worth noting that these conclusions hold true for two systems very much similar in terms of comparison with the experimental total structure factor and yet quite different when focussing on the local network organization (as shown by the percentages of tetrahedral *vs* octahedral structural motifs).

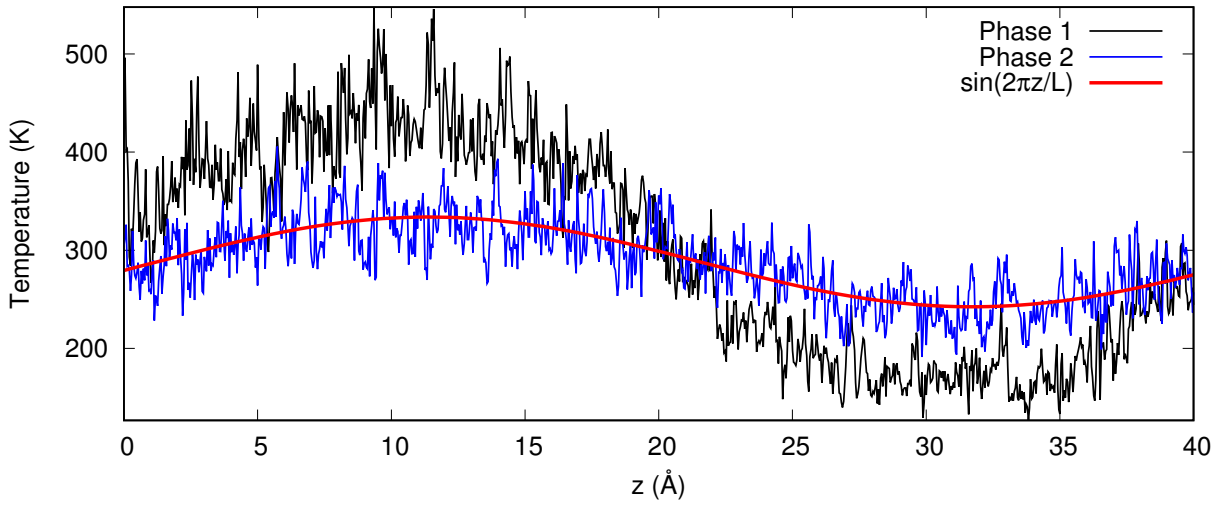

FIG. 8. Temperature profiles averaged during phase 1 (black curve) and phase 2 (blue curve) and fit by a sinusoidal variation in phase 2 (red curve). AEMD of the 504-GTH model.

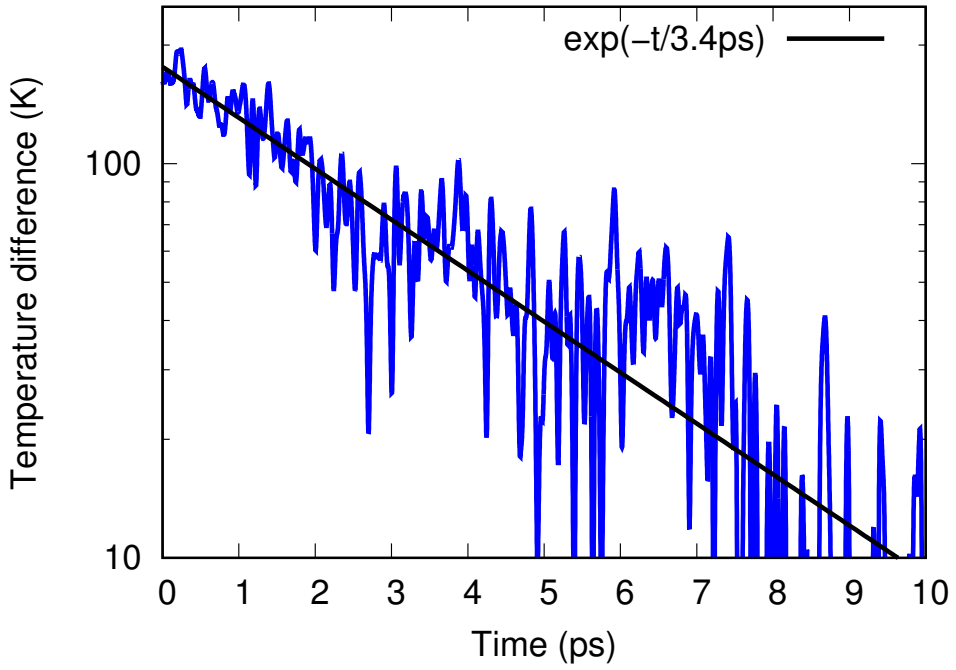

FIG. 9. Temperature difference between the hot and cold blocks during phase 2 (blue line) and exponential fit to extract the transient time τ (here equal to 3.4 ps). Data refer to the 504-GTH model.

TABLE VI. Transient times τ and thermal conductivities κ obtained in the 504-TM and 504-GTH models.

	504-TM		504-GTH	
	τ (ps)	κ (W K^{-1} m^{-1})	τ (ps)	κ (W K^{-1} m^{-1})
1stAEMD	6.1	0.12	5.0	0.12
2ndAEMD	6.2	0.11	3.4	0.17
3rdAEMD	6.0	0.12	5.2	0.11
Average		0.12±0.01		0.13±0.03

VI. CONCLUSION

The establishment of a correlation between atomic structure and thermal properties presented in this work has been done on the basis of two DFT-FPMD model of amorphous $Ge_2Sb_2Te_5$, differing only in the type of PP used for the core-valence interaction. In Ref. 13 we demonstrated that the best agreement with neutron scattering data was obtained for the Trouiller-Martins (TM)[17] PP, in conjunction with appropriate choices for the local and non local part of the Ge PP. We had also shown, and confirmed in the present work for a larger simulation box (N= 504), that the

GST network topology issued by the TM model favors the predominance of Ge tetrahedrally coordinated, unlike the atomic structure obtained via the alternative GTH PP construction.[18]

The existence of two legitimate models for *a*GST has opened the way to a study of the sensitivity to the network atomic structure of the thermal conductivity κ. Recent FPMD-AEMD studies[8] have demonstrated a sizeable reduction of κ in the nanoscale regime and a correct asymptotic behavior to the bulk value. As a first information on vibrational properties, we have calculated the corresponding density of states, exhibiting a more important tail at higher frequencies in the TM case. This change is not reflected by the values of the thermal conductivity that are found insensitive to the relative proportion of tetrahedral *vs* octahedral structural units. We can conclude that extended mode of vibrations, responsible for changes of thermal conductivity in the nanoscale range, are not affected by local variations in the atomic structure as those found when comparing TM and GTH models.

ACKNOWLEDGEMENTS

This work was funded by the French ANR via the project n. ANR-17-CE09-0039-02 “SIRENA". Calculations were performed by using resources from GENCI (Grand Equipement National de Calcul Intensif) (Grants No. 0910296 and 0905071). The authors would like to acknowledge the High Performance Computing Center of the University of Strasbourg for supporting this work by providing scientific support and access to computing resources. Part of the computing resources were funded by the Equipex Equip@Meso project (Programme Investissements d’Avenir) and the CPER Alsacalcul/Big Data.

AUTHOR DECLARATIONS

The authors have no conflicts to disclose.

DATA AVAILABILITY STATEMENT

The data that support the findings of this study are available from the corresponding author upon reasonable request.

REFERENCES

[1]A. S. Henry, G. Chen, Spectral Phonon Transport Properties of Silicon Based on Molecular Dynamics Simulations and Lattice Dynamics (Feb. 2008). doi:info:doi/10.1166/jctn.2008.2454.

[2]K. T. Regner, D. P. Sellan, Z. Su, C. H. Amon, A. J. McGaughey, J. A. Malen, Broadband phonon mean free path contributions to thermal conductivity measured using frequency domain thermoreflectance, Nature Communications 4 (2013) 1640. doi:10.1038/ncomms2630.

[3]F. X. Alvarez, D. Jou, Memory and nonlocal effects in heat transport: From diffusive to ballistic regimes, Applied Physics Letters 90 (8) (2007) 083109. doi:10.1063/1.2645110.

[4]P. L. Palla, S. Zampa, E. Martin, F. Cleri, Interface thermal behavior in nanomaterials by thermal grating relaxation, International Journal of Heat and Mass Transfer 131 (2019) 932–943. doi:10.1016/j.ijheatmasstransfer.2018.11.064.

[5]M. C. Wingert, J. Zheng, S. Kwon, R. Chen, Thermal transport in amorphous materials: A review, Semiconductor Science and Technology 31 (11) (2016) 113003. doi:10.1088/0268-1242/31/11/113003.

[6]Y. He, D. Donadio, G. Galli, Heat transport in amorphous silicon: Interplay between morphology and disorder, Applied Physics Letters 98 (14) (2011) 144101. doi:10.1063/1.3574366.

[7]T.-Q. Duong, C. Massobrio, G. Ori, M. Boero, E. Martin, Thermal conductivity and transport modes in glassy $GeTe_4$ by first-principles molecular dynamics, Physical Review Materials 3 (10) (2019) 105401. doi:10.1103/PhysRevMaterials.3.105401.

[8]T.-Q. Duong, A. Bouzid, C. Massobrio, G. Ori, M. Boero, E. Martin, First-principles thermal transport in amorphous $Ge_2Sb_2Te_5$ at the nanoscale, RSC Advances 11 (18) (2021) 10747–10752. doi:10.1039/D0RA10408F.

[9]E. Martin, G. Ori, T.-Q. Duong, M. Boero, C. Massobrio, Thermal conductivity of amorphous SiO_2 by first-principles molecular dynamics, Journal of Non-Crystalline Solids 581 (2022) 121434. doi:10.1016/j.jnoncrysol.2022.121434.

[10]P. B. Allen, J. L. Feldman, J. Fabian, F. Wooten, Diffusons, locons and propagons: Character of atomie yibrations in amorphous Si, Philosophical Magazine B 79 (11-12) (1999) 1715–1731. doi:10.1080/13642819908223054.

[11]V. Joshi, M. Le Gallo, S. Haefeli, I. Boybat, S. R. Nandakumar, C. Piveteau, M. Dazzi, B. Rajendran, A. Sebastian, E. Eleftheriou, Accurate deep neural network inference using compu-

tational phase-change memory, Nature Communications 11 (1) (2020) 2473. doi:10.1038/s41467-020-16108-9.

[12]L. Berguiga, L. Ferrier, C. Jamois, T. Benyattou, X. Letartre, S. Cueff, Ultimate phase sensitivity in surface plasmon resonance sensors by tuning critical coupling with phase change materials, Optics Express 29 (25) (2021) 42162–42175. doi:10.1364/OE.439869.

[13]A. Bouzid, G. Ori, M. Boero, E. Lampin, C. Massobrio, Atomic-scale structure of the glassy $Ge_2Sb_2Te_5$ phase change material: A quantitative assessment via first-principles molecular dynamics, Physical Review B 96 (22) (2017) 224204. doi:10.1103/PhysRevB.96.224204.

[14]J. P. Perdew, K. Burke, M. Ernzerhof, Generalized gradient approximation made simple, Phys. Rev. Lett. 77 (1996) 3865–3868. doi:10.1103/PhysRevLett.77.3865.

[15]A. D. Becke, Density-functional exchange-energy approximation with correct asymptotic behavior, Physical Review A 38 (6) (1988) 3098–3100. doi:10.1103/PhysRevA.38.3098.

[16]C. Lee, W. Yang, R. G. Parr, Development of the Colle-Salvetti correlation-energy formula into a functional of the electron density, Physical Review B 37 (2) (1988) 785–789. doi:10.1103/PhysRevB.37.785.

[17]N. Troullier, J. L. Martins, Efficient pseudopotentials for plane-wave calculations, Physical Review B 43 (3) (1991) 1993–2006. doi:10.1103/PhysRevB.43.1993.

[18]S. Goedecker, M. Teter, J. Hutter, Separable dual-space Gaussian pseudopotentials, Physical Review B 54 (3) (1996) 1703–1710. doi:10.1103/PhysRevB.54.1703.

[19]J. Akola, R. O. Jones, Density functional study of amorphous, liquid and crystalline $Ge_2Sb_2Te_5$: homopolar bonds and/or ab alternation?, Journal of Physics: Condensed Matter 20 (46) (2008) 465103. doi:10.1088/0953-8984/20/46/465103.

[20]J. Akola, R. O. Jones, Structural phase transitions on the nanoscale: The crucial pattern in the phase-change materials $Ge_2Sb_2Te_5$ and GeTe, Phys. Rev. B 76 (2007) 235201. doi:10.1103/PhysRevB.76.235201.

[21]S. Caravati, M. Bernasconi, T. D. Kühne, M. Krack, M. Parrinello, Coexistence of tetrahedral- and octahedral-like sites in amorphous phase change materials, Applied Physics Letters 91 (17) (2007) 171906. arXiv:https://doi.org/10.1063/1.2801626, doi:10.1063/1.2801626. URL https://doi.org/10.1063/1.2801626

[22]S. Caravati, M. Bernasconi, T. D. Kühne, M. Krack, M. Parrinello, First-principles study of crystalline and amorphous $Ge_2Sb_2Te_5$ and the effects of stoichiometric defects, Journal of Physics: Condensed Matter 21 (25) (2009) 255501. doi:10.1088/0953-8984/21/25/255501.

[23]B. Cai, D. A. Drabold, S. R. Elliott, Structural fingerprints of electronic change in the phase-change-material: $Ge_2Sb_2Te_5$, Applied Physics Letters 97 (19) (2010) 191908. doi:10.1063/1.3516039.

[24]J. Hegedüs, S. R. Elliott, Microscopic origin of the fast crystallization ability of Ge-Sb-Te phase-change memory materials, Nature Materials 7 (2008) 399. doi:10.1038/nmat2157.

[25]G. C. Sosso, S. Caravati, R. Mazzarello, M. Bernasconi, Raman spectra of cubic and amorphous $Ge_2Sb_2Te_5$ from first principles, Phys. Rev. B 83 (2011) 134201. doi:10.1103/PhysRevB.83.134201.

[26]C. Lang, S. A. Song, D. N. Manh, D. J. H. Cockayne, Building blocks of amorphous $Ge_2Sb_2Te_5$, Phys. Rev. B 76 (2007) 054101. doi:10.1103/PhysRevB.76.054101.

[27]J. Akola, R. O. Jones, S. Kohara, S. Kimura, K. Kobayashi, M. Takata, T. Matsunaga, R. Kojima, N. Yamada, Experimentally constrained density-functional calculations of the amorphous structure of the prototypical phase-change material $Ge_2Sb_2Te_5$, Phys. Rev. B 80 (2009) 020201. doi:10.1103/PhysRevB.80.020201.

[28]J. Akola, R. O. Jones, Amorphous structures of Ge/Sb/Te alloys: Density functional simulations, Physica Status Solidi (b) 249 (10) (2012) 1851–1860. doi:10.1002/pssb.201200393.

[29]S. Caravati, M. Bernasconi, Influence of the exchange and correlation functional on the structure of amorphous, Physica Status Solidi (b) 252 (2) (2015) 260–266. doi:10.1002/pssb.201451441.

[30]F. C. Mocanu, K. Konstantinou, T. H. Lee, N. Bernstein, V. L. Deringer, G. Csányi, S. R. Elliott, Modeling the Phase-Change Memory Material, $Ge_2Sb_2Te_5$, with a Machine-Learned Interatomic Potential, The Journal of Physical Chemistry B 122 (38) (2018) 8998–9006. doi:10.1021/acs.jpcb.8b06476.

[31]T. H. Lee, S. R. Elliott, The relation between chemical bonding and ultrafast crystal growth, Advanced Materials 29 (24) (2017) 1700814. doi:https://doi.org/10.1002/adma.201700814.

[32]A. V. Kolobov, P. Fons, A. I. Frenkel, A. L. Ankudinov, J. Tominaga, T. Uruga, Understanding the phase-change mechanism of rewritable optical media, Nature Materials 3 (10) (2004) 703–708. doi:10.1038/nmat1215.

[33]D. A. Baker, M. A. Paesler, G. Lucovsky, S. C. Agarwal, P. C. Taylor, Application of Bond Constraint Theory to the Switchable Optical Memory Material $Ge_2Sb_2Te_5$, Physical Review Letters 96 (25) (2006) 255501. doi:10.1103/PhysRevLett.96.255501.

[34]S. Hosokawa, T. Ozaki, K. Hayashi, N. Happo, M. Fujiwara, K. Horii, P. Fons, A. V. Kolobov, J. Tominaga, Existence of tetrahedral site symmetry about Ge atoms in a single-crystal film of $Ge_2Sb_2Te_5$ found by x-ray fluorescence holography, Applied Physics Letters 90 (13) (2007) 131913. doi:10.1063/1.2717094.

[35]P. Jóvári, I. Kaban, J. Steiner, B. Beuneu, A. Schöps, A. Webb, 'wrong bonds' in sputtered amorphous $Ge_2Sb_2Te_5$, Journal of Physics: Condensed Matter 19 (33) (2007) 335212. doi:10.1088/0953-8984/19/33/335212.

[36]J. Akola, J. Larrucea, R. O. Jones, Polymorphism in phase-change materials: melt-quenched and as-deposited amorphous structures in $Ge_2Sb_2Te_5$ from density functional calculations, Phys. Rev. B 83 (2011) 094113. doi:10.1103/PhysRevB.83.094113.

[37]S. Hosokawa, W.-C. Pilgrim, A. Höhle, D. Szubrin, N. Boudet, J.-F. Bérar, K. Maruyama, Key experimental information on intermediate-range atomic structures in amorphous $Ge_2Sb_2Te_5$ phase change material, Journal of Applied Physics 111 (8) (2012) 083517. doi:10.1063/1.3703570.

[38]M. Micoulaut, A. Piarristeguy, H. Flores-Ruiz, A. Pradel, Towards accurate models for amorphous GeTe: Crucial effect of dispersive van der Waals corrections on the structural properties involved in the phase-change mechanism, Phys. Rev. B 96 (2017) 184204. doi:10.1103/PhysRevB.96.184204.

[39]M. Cobelli, D. Dragoni, S. Caravati, M. Bernasconi, Metal-semiconductor transition in the supercooled liquid phase of the $Ge_2Sb_2Te_5$ and GeTe compounds, Phys. Rev. Mater. 5 (2021) 045004. doi:10.1103/PhysRevMaterials.5.045004.

[40]O. Abou El Kheir, D. Dragoni, M. Bernasconi, Density functional simulations of decomposition pathways of Ge-rich GeSbTe alloys for phase change memories, Phys. Rev. Mater. 5 (2021) 095004. doi:10.1103/PhysRevMaterials.5.095004.

[41]S. Perego, D. Dragoni, S. Gabardi, D. Campi, M. Bernasconi, Structure and crystallization kinetics of as-deposited films of the GeTe phase change compound from atomistic simulations, Physica Status Solidi (RRL) – Rapid Research Letters 2200433doi:10.1002/pssr.202200433.

[42]R. Car, M. Parrinello, Unified Approach for Molecular Dynamics and Density-Functional Theory, Physical Review Letters 55 (22) (1985) 2471–2474. doi:10.1103/PhysRevLett.55.2471.

[43]Jointly by IBM Corporation and by Max Planck Institute, Stuttgart, CPMD code (2021). URL http://www.cpmd.org

[44]S. Nosé, A molecular dynamics method for simulations in the canonical ensemble, Molecular Physics 52 (2) (1984) 255–268. doi:10.1080/00268978400101201.

[45]S. Nosé, A unified formulation of the constant temperature molecular dynamics methods, The Journal of Chemical Physics 81 (1) (1984) 511–519. doi:10.1063/1.447334.

[46]W. G. Hoover, Canonical dynamics: Equilibrium phase-space distributions, Physical Review A 31 (3) (1985) 1695–1697. doi:10.1103/PhysRevA.31.1695.

[47]G. J. Martyna, M. L. Klein, M. Tuckerman, Nosé–Hoover chains: The canonical ensemble via continuous dynamics, The Journal of Chemical Physics 97 (4) (1992) 2635–2643. doi:10.1063/1.463940.

[48]P. E. Blöchl, M. Parrinello, Adiabaticity in first-principles molecular dynamics, Physical Review B 45 (16) (1992) 9413–9416. doi:10.1103/PhysRevB.45.9413.

[49]A. V. Kolobov, P. Fons, A. I. Frenkel, A. L. Ankudinov, J. Tominaga, T. Uruga, Understanding the phase-change mechanism of rewritable optical media, Nature Materials 3 (10) (2004) 703–708. doi:10.1038/nmat1215.

[50]D. A. Baker, M. A. Paesler, G. Lucovsky, S. C. Agarwal, P. C. Taylor, Application of Bond Constraint Theory to the Switchable Optical Memory Material $Ge_2Sb_2Te_5$, Physical Review Letters 96 (25) (2006) 255501. doi:10.1103/PhysRevLett.96.255501.

[51]J. R. Errington, P. G. Debenedetti, Relationship between structural order and the anomalies of liquid water, Nature 409 (6818) (2001) 318–321. doi:10.1038/35053024.

[52]S. Le Roux, P. Jund, Ring statistics analysis of topological networks: New approach and application to amorphous GeS_2 and SiO_2 systems, Computational Materials Science 49 (1) (2010) 70–83. doi:10.1016/j.commatsci.2010.04.023.

[53]A. C. Wright, R. N. Sinclair, A. J. Leadbetter, Effect of preparation method on the structure of amorphous solids in the system As-S, Journal of Non-Crystalline Solids 71 (1) (1985) 295–302. doi:10.1016/0022-3093(85)90299-6.

[54]R. J. Bell, P. Dean, D. C. Hibbins-Butler, Localization of normal modes in vitreous silica, germania and beryllium fluoride, Journal of Physics C: Solid State Physics 3 (10) (1970) 2111–2118.

[55]B. B. Laird, H. R. Schober, Localized low-frequency vibrational modes in a simple model glass, Phys. Rev. Lett. 66 (1991) 636–639. doi:10.1103/PhysRevLett.66.636.

[56]A. Bouzid, H. Zaoui, P. L. Palla, G. Ori, M. Boero, C. Massobrio, F. Cleri, E. Lampin, Thermal conductivity of glassy $GeTe_4$ by first-principles molecular dynamics, Physical Chemistry Chemical Physics 19 (15) (2017) 9729–9732. doi:10.1039/C7CP01063J.

[57]T.-Q. Duong, C. Massobrio, M. Boero, G. Ori, E. Martin, Heat transport in disordered network forming materials: Size effects and existence of propagative modes, Computational Materials Science 177 (2020) 109607. doi:10.1016/j.commatsci.2020.109607.